Design and Testing of a Blended Wing Body Aeroelastic Wind-Tunnel Model

Martin Carlsson* and Jakob Kuttenkeuler†
Kungliga Tekniska Högskolan,
SE-100 44 Stockholm, Sweden

Introduction

ELASTIC wind tunnel models are frequently used to validate performance and aeroelastic behavior of full size aircraft structures, for example, see Sensburg et al.,[1] Schneider et al.[2] and Baker et al.[3] The model usually represents a full-size structure in an aeroelastically scaled sense. Techniques based on numerical optimization are sometimes used to achieve representative model behavior. For example, French and Eastep[4] present an approach for matching both static and dynamic aeroelastic properties. Once manufactured, the stiffness properties of the model are usually fixed, but the mass distribution may be modified by adding masses at various locations. Modular elastic models, for which the stiffness and mass properties can be changed, are also being developed and are used for multipurpose investigations, for example, see Amiryants and Ishmuratov.[5]

Both the manufacturing and the experimental testing of aeroelastic wind-tunnel models can be very complicated due to the complexity of the models and the equipment required for aeroelastic measurements. This study focuses on an experimental approach that allows for short design and testing cycles using limited resources. Hence, experimental data for validation purposes can be delivered at a very early phase of a new project. The aim is to use a relatively simple modular aeroelastic model in combination with more sophisticated, yet easy to use, experimental equipment for data acquisition.

For validation of aeroelastic analysis, access to experimental data in terms of both aerodynamic loads and aeroelastic deformations is normally required. Whereas load measurements are routinely performed using various types of wind-tunnel balances, the concern of deformation measurements is usually more involved. In the present study, an optical technique based on multiple-camera photogrammetry is used in combination with passive reflecting markers attached to the model. One significant advantage with passive-type markers is that no cabling inside the model is required, hence, further simplifying the model manufacturing and testing. Experiments using multiple-camera photogrammetry and passive markers have also been conducted at NASA, as reported by Burner and Liu.[6]

The particular wind tunnel model considered in this paper is designed for low-speed aeroelastic investigations of a Blended Wing Body (BWB) transport aircraft. The BWB type of nonconventional subsonic transport concept has been the objective for several studies concerning potential benefits compared to more conventional aircraft. An overview of the BWB concept and promising results are presented by Roman et al.[7] and Liebeck et al.[8]

One important issue with the study of the BWB concept is that tools for analysis of conventional aircraft have been developed for decades, although the development of the BWB provides new challenges. This implies that verification of numerical results, by using, for example, wind-tunnel models, becomes very important.

Received 25 February 2002; revision received 27 September 2002; accepted for publication 5 October 2002.

*Ph.D. Student, Department of Aeronautics, Division of Flight Dynamics, Teknikringen 8. Member AIAA.

†Senior Lecturer, Department of Aeronautics, Division of Flight Dynamics, Teknikringen 8.

Model Design

The requirements on aeroelastic wind-tunnel models are dictated by the type of experimental investigations to be made. The models are consequently tailored for a specific type of investigation.[9] In the present study, the design has been simplified as compared to the full-size structure to limit the manufacturing time and cost. Hence, scaling of the aircraft internal structure is eliminated. Furthermore, the ability to change the model stiffness and mass properties is required. To meet this requirement, the model is built in a modular fashion.

To increase the size of the structure and to simplify manufacturing, the semispan model approach is chosen. This concept is often used as the Reynolds number is increased compared to when using a full-span model for a given wind-tunnel size.[10] The planform is chosen to represent a typical BWB aircraft, although the geometry is slightly simplified. For example, the airfoil is symmetric and thicker than what would normally be used for the full-scale aircraft to allow space for equipment inside the model. Furthermore, to reduce the manufacturing time and cost, there are no double-curved surfaces. The resulting geometry of the wind-tunnel model is shown in Fig. 1.

Although the model is designed for aeroelastic testing, the inner part, referred to as the fuselage, is rigid, whereas the outer part of the model is elastic. The elastic part of the model is designed using the segmented concept, which is often used for low-speed elastic wind-tunnel models.[9] The stiffness of the model is related to the properties of an internal carbon fiber/epoxy composite beam used for primary structure support. By the use of this approach, the elastic behavior of the model can be tailored by varying the beam composite layup and geometry. Furthermore, the beam can easily be replaced for testing of various stiffness properties.

The outer aerodynamic shape is achieved using stiff wing sections clamped to the composite beam. The wing sections are separated by small gaps to allow for individual movement without interference. For low-speed testing, such small gaps have minimal influence on the out-of-plane aerodynamic loads.[11] However, the aerodynamic drag will most likely be affected by the gaps, and therefore, the model is not suitable for drag estimations. Both the fuselage and the stiff wing sections are made of foam core covered with polymer composite faces. This results in a lightweight, yet stiff, design.

Finally, a six-component balance is used to measure the loads acting on the elastic part of the model. The balance is mounted in the volume of the fuselage as shown in Fig. 1.

Numerical Modeling

The wind-tunnel model will be used for validation of various numerical representations. However, a very common approach for low-speed aeroelastic investigations is to combine a finite element structural model[12] with doublet lattice aerodynamics.[13] Hence, such a numerical model is chosen for the initial validation experiments.

The structural modeling is rather simple because the wing beam is the only elastic member. The beam is modeled using eight-node shell elements with anisotropic material properties. Convergence

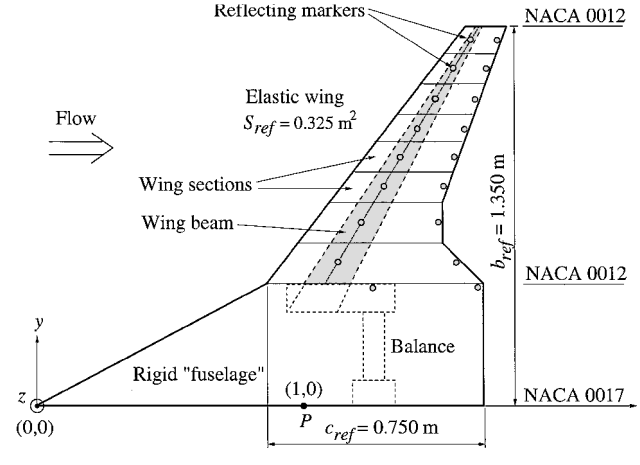

Fig. 1 BWB wind-tunnel model.

studies, with respect to the beam eigenfrequencies, were performed to determine the required mesh density. It was concluded that 192 elements (4 chordwise times 48 spanwise) were sufficient to represent the wing beam. The stiff wing sections are structurally modeled as rigid bodies connected to the beam at the points of physical attachment. The mass properties of the wing sections are experimentally determined using a mass moment of inertia instrument.

Considering the aerodynamics, each stiff wing section is modeled as one separate panel containing 10 chordwise times 4 spanwise aerodynamic boxes. The aerodynamic boxes of each panel are then coupled to the motion of the corresponding rigid body representing the wing section using spline functions. Also the fuselage is represented by one panel containing 10 times 4 aerodynamic boxes. Furthermore, the aerodynamic model is made symmetric around the model centerline to account for the wind-tunnel boundary.

Experimental Setup

All testing was performed in a low-speed wind tunnel at the Royal Institute of Technology (KTH). The cross section of the 3.6 m^2 test section is quadratic with corner fillets. The environmental test conditions were room temperature and atmospheric pressure. Therefore, standard sea-level atmospheric conditions were used in all conversions between dynamic pressure q and airspeed u.

The inner rigid part of the model was attached to a servocontrolled turntable in the wind-tunnel floor. The root of the balance was bolted to the turntable, and the outer end was attached to a wing beam clamping device. Thus, all loads acting on the elastic part of the model were transferred through the balance into the wind-tunnel turntable.

The elastic deformations are measured using an optical positioning system mounted in the wind tunnel.[14,15] Figure 1 shows the position of reflecting markers attached to the model for deformation measurements. The optical system consists of a host computer and four infrared charge-coupled device cameras with internal flashes, interconnected in a local network. Within each camera, the two-dimensional optical centers of all visible markers are calculated. The two-dimensional positions are then transferred from each camera to the host computer where the three-dimensional photogrammetric calculations are performed. The present system works at frame rates up to 240 Hz and has a three-dimensional resolution on the order of 0.03 mm for the setup used for this investigation. When the marker setup shown in Fig. 1 is used, this corresponds to about 0.025-deg resolution in torsional deformation.

Results and Discussion

To validate the numerical model of the structure, the natural frequencies of the model were calculated and compared to experimental results. The experimentally measured frequencies were obtained by vibration testing using accelerometers mounted at various model locations. The agreement between the frequencies was good, which indicated that the numerical model was representative concerning both stiffness and mass properties. Also, the result indicated that the model was manufactured according to the requirements considering stiffness and mass properties. Note that no adjustments or updating of material properties were performed to make the numerical results match experimental data.

Static aerodynamic loads are measured at various flow speeds u and root angle of attack α ranging from -5 to 10 deg. The loads are given relative to the reference point P at $(x, y, z) = (1, 0, 0)$ (Fig. 1) in the body-fixed system. Furthermore, the loads are normalized according to

$$C_{F_z} = F_z/qS_{\text{ref}}, \qquad C_{M_y} = M_y/qS_{\text{ref}}c_{\text{ref}}$$
$$C_{M_x} = M_x/qS_{\text{ref}}b_{\text{ref}} \tag{1}$$

where C_{F_z}, C_{M_y}, and C_{M_x} are the normalized coefficient of the force in the z direction, F_z, the moment around the y axis, M_y, and the moment around the x axis, M_x, respectively. The reference area is represented by S_{ref}, and c_{ref} is the reference chord and b_{ref} the reference span. Because only loads on the elastic part of the model are considered, the area of this part is used as the reference area (Fig. 1). Figure 1 also shows the definition of reference chord and reference span.

Table 1 Aerodynamic derivatives at $u = 25$ m/s

Aerodynamic derivative	Prediction, rad^{-1}	Experiment, rad^{-1}	|(exp − pred)/exp|, %
$\partial C_{F_z}/\partial\alpha$	4.34	4.65	6.7
$\partial C_{M_y}/\partial\alpha$	−1.62	−1.74	6.9
$\partial C_{M_x}/\partial\alpha$	2.59	2.79	7.2

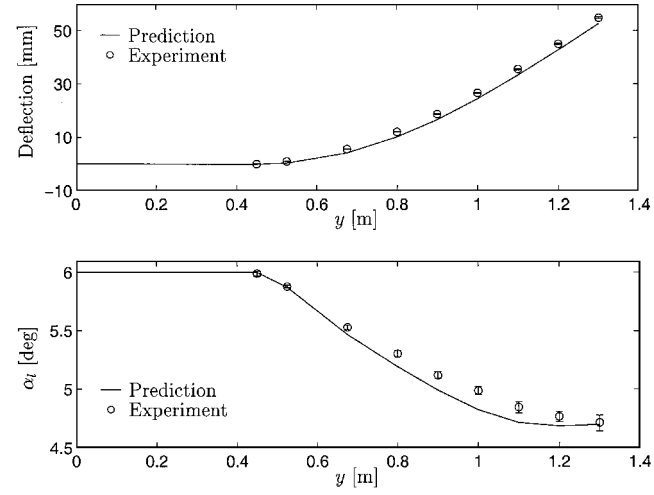

Fig. 2 Model deformations at $u = 25$ m/s and $\alpha = 6$ deg.

The measured aerodynamic derivatives with respect to α are compared to numerical results in Table 1. As shown, the correlation between the numerical predictions and the measured loads is good, although the experimentally measured aerodynamic derivatives are overall somewhat higher in magnitude.

At the same conditions at which the loads are measured, the aeroelastic deformations of the model are measured using the optical positioning system. A comparison between numerically predicted wing deformations and corresponding measured values at $u = 25$ m/s and $\alpha = 6$ deg is presented in Fig. 2. Here, wing deflection refers to the out-of-plane displacement at the beam centerline, which is measured at 10 spanwise positions. The wing elastic twist is presented as local angle of attack α_l, at the same spanwise locations. According to Fig. 2, the numerical prediction agrees fairly well with the measured deformations. The wing sweep, in combination with the position of the elastic axis, results in a decrease of the local angle of attack toward the tip as expected and as predicted by the numerical model. However, the experiment shows that the elastic wing twist is slightly smaller than predicted, hence, resulting in a spanwise consistent higher α_l. This can explain why the measured loads are somewhat higher than predicted.

When performing the optical measurements, the positions of the markers are sampled at 100 Hz during 10 s. The wing deformations are calculated from all samples, and the mean values are used to represent the experimentally measured deformations. Although the test is treated as static, there are always small disturbances in the wind-tunnel flow, which make it very dubious to calculate the deformation of the wing with respect to only one single camera sample, especially when the measured deformations are small. The bars in Fig. 2 show the range in which the measured deformations are varied within the test sequence of 10 s. The variations in wing deflection are relatively small. The wing tip deflection varies within a 0.7-mm range. However, the twist variations are more evident. At the tip of the model, the torsional deformation varies by 0.14 deg, which is about 11% of the total measured elastic twist at the tip.

Conclusions

Despite the quite simple design concept, the elastic wind-tunnel model is shown to be well suited for low-speed aeroelastic investigations. Furthermore, the segmented concept enables the possibility to replace individual wing sections. For example, new wing sections including control surfaces can easily be used for studies regarding control surface efficiency and aeroservoelastic response. Moreover, it is possible to design various internal wing beams with different stiffness properties for experimental comparison of aeroelastic performance on a model level. Also, new masses can be added to the individual wing sections to modify the dynamic behavior of the model.

When the experimental procedure, including both model manufacturing and wind-tunnel testing is considered, the study shows that the use of a relatively simple model concept can be very useful to provide experimental information at an early stage of a new project. The efficiency of the experimental testing is further increased as the experimental setup including load and deformation measurements as well as wind-tunnel operation can be handled by a single operator. Especially, the use of the optical positioning system in combination with passive reflecting markers for deformation measurements is shown to be very efficient.

Finally, the development of the BWB concept provides many new challenges. However, the results from this study indicate that standard numerical tools are capable of predicting the low-speed aeroelastic behavior of the BWB planform with reasonable accuracy.

Acknowledgments

This work was financially supported by the Commission of the European Union. The investigation was carried out within the project Multi-Disciplinary Design and Optimisation for Blended Wing Body Configuration, Contract G4RD-CT1999-0172.

References

[1]Sensburg, O., Schweiger, J., Tischler, V. A., and Venkayya, V. B., "Aeroelastic Tailoring of Aerodynamic Surfaces and Low Cost Wind Tunnel Model Design," *Proceedings of the International Workshop on Multidisciplinary Design Optimization*, Rept. ADA 389797, Pretoria, South Africa, 2000, pp. 240–253.

[2]Schneider, G., Hoenlinger, H., Guldner, W., and Manser, R., "Aeroelastic Tailoring Validation by Windtunnel Model Testing," *Proceedings of the European Forum on Aeroelasticity and Structural Dynamics*, Deutsche Gesellschaft Fuer Luft- und Raumfahrt, Bonn, Germany, 1989, pp. 399–408.

[3]Baker, M. L., Mendoza, R., and Hartwich, P. M., "Transonic Aeroelastic Analysis of a High Speed Transport Wind-Tunnel Model," AIAA Paper 99-1217, April 1999.

[4]French, M., and Eastep, F. E., "Aeroelastic Model Design Using Parameter Identification," *Journal of Aircraft*, Vol. 33, No. 1, 1996, pp. 198–202.

[5]Amiryants, G. A., and Ishmuratov, F. Z., "Multi-Purpose Modular Aerodynamic/Aeroelastic Model," *Proceedings of the CEAS/AIAA/AIAE International Forum on Aeroelasticity and Structural Dynamics*, Madrid, Spain, Vol. 3, June 2001, pp. 509–518.

[6]Burner, A. W., and Liu, T., "Videogrammetric Model Deformation Measurement Technique," *Journal of Aircraft*, Vol. 38, No. 4, 2001, pp. 745–754.

[7]Roman, D., Allen, J. B., and Liebeck, R. H., "Aerodynamic Design Challenges of the Blended-Wing–Body Subsonic Transport," AIAA Paper 2000-4335, Aug. 2000.

[8]Liebeck, R. H., Page, M. A., and Rawdon, B. K., "Blended-Wing–Body Subsonic Commercial Transport," AIAA Paper 98-0438, Jan. 1998.

[9]Barlow, J. B., Rae, W. H., and Pope, A., *Low-Speed Wind Tunnel Testing*, 3rd ed., Wiley, New York, 1999, pp. 683–691.

[10]Milholen, W. E., II, and Chokani, N., "Development of Semispan Model Test Techniques," *Journal of Aircraft*, Vol. 33, No. 6, 1996, pp. 1115–1122.

[11]Carlsson, M., "Aeroelastic Testing of a Sectioned Wind Tunnel Model," Dept. of Aeronautics, Rept. C2000-06, Royal Inst. of Technology, Stockholm, June 2000.

[12]Rodden, W. P., and Johnson, E. H., "MSC/NASTRAN Aeroelastic Analysis Users Guide," Ver. 68, MacNeal–Schwendler, Los Angeles, Oct. 1994.

[13]Albano, E., and Rodden, W. P., "A Doublet-Lattice Method for Calculating Lift Distributions on Oscillating Surfaces in Subsonic Flows," *AIAA Journal*, Vol. 7, No. 2, 1969, pp. 279–285.

[14]Qualisys, A. B., "ProReflex," Ver. 6.41, Technical Reference, Sävedalen, Sweden, 1997.

[15]Kuttenkeuler, J., and Carlsson, M., "Optical Deformation Measurements in Wind Tunnel Testing," *Proceedings of the CEAS/AIAA/AIAE International Forum on Aeroelasticity and Structural Dynamics*, Madrid, Spain, Vol. 3, June 2001, pp. 499–508.

Mixed Jameson/Total-Variation-Diminishing Scheme Applied to Simulating Rotor Airfoil Flowfield

Yihua Cao,* Jifei Wang,† and Yuan Su‡
Beijing University of Aeronautics and Astronautics, Beijing 100083, People's Republic of China

Introduction

WITH the rapid development of computational technology, numerical simulation by solving classical governing equations of fluid dynamics is playing a more and more important role in air vehicle aerodynamics, specifically in rotorcraft aerodynamics (Ref. 1). To date, various computational methods have been investigated, and the finite volume central differential scheme created by Jameson et al.[2] has been demonstrated to be a robust method and has been widely used in computational rotor aerodynamics. More recently, many high-resolution schemes are emerging, for example, the total-variation-diminishing (TVD) scheme[3,4] is a representative one.

In this Note, a classical rotor airfoil (NACA0012) has been chosen as the example to demonstrate the flexibility of a mixed Jameson/TVD scheme in computational rotor aerodynamics. At first, Jameson's finite volume central differential scheme is implemented to solve the Euler equations describing the flowfield around the airfoil just mentioned. Then, a mixed Jameson/TVD scheme is constructed by correcting artificial viscous terms to capture the position of the shock wave more precisely. Also, for the first time this scheme is used to solve the Euler equations for the simulation of the flowfield around a rotor airfoil. Additionally, with regard to the Euler equations' deficiency in reflecting viscous effects, Jameson's scheme is applied to solve the turbulent Navier–Stokes (N–S) equations, which is a good start for further numerical calculation of helicopter rotor drag force and power.

Governing Equations

For two-dimensional problems the compressible N–S equations can be represented in the following conservation form:

$$\frac{\partial W}{\partial t}+\frac{\partial F}{\partial x}+\frac{\partial G}{\partial y}=\frac{\partial R}{\partial x}+\frac{\partial S}{\partial y} \tag{1}$$

where

$$W=\begin{bmatrix}\rho\\ \rho u\\ \rho v\\ \rho e\end{bmatrix}\quad F=\begin{bmatrix}\rho u\\ \rho u^2+p\\ \rho uv\\ \rho uh\end{bmatrix}\quad G=\begin{bmatrix}\rho v\\ \rho uv\\ \rho v^2+p\\ \rho vh\end{bmatrix}$$

Received 31 May 2002; revision received 22 September 2002; accepted for publication 27 September 2002.

*Professor, Department of Flight Vehicle Design and Applied Mechanics.
†Doctor, Department of Flight Vehicle Design and Applied Mechanics.
‡Lecturer, Department of Flight Vehicle Design and Applied Mechanics.